YMTHE, Volume *31*

Supplemental Information

Polyphyllin D punctures hypertrophic lysosomes to reverse drug resistance of hepatocellular carcinoma by targeting acid sphingomyelinase

Yang Wang, Yan-Yan Chen, Gui-Bin Gao, Yang-Han Zheng, Nan-Nan Yu, Lan Ouyang, Xuejuan Gao, Nan Li, Shi-Yuan Wen, Shangjia Huang, Qian Zhao, Langxia Liu, Mingrong Cao, Shuixing Zhang, Jing Zhang, and Qing-Yu He

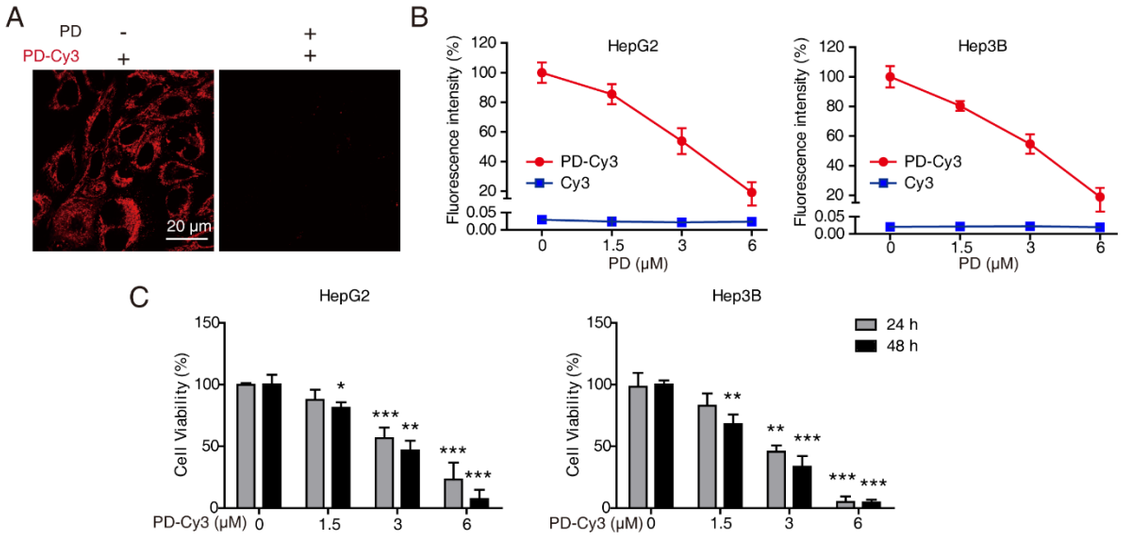

Figure S1. Characterization of PD-Cy3. (A) HepG2 cells stained with PD-Cy3 were observed under confocal microscopy with or without pre-treated with PD (6 μM). (B) Binding affinity of PD to lysosome was assessed using a fluorescence competition assay. After pretreated with PD at various concentrations (0-6 μM), fluorescence intensity of PD-Cy3 loaded HCC cells was determined by flow cytometry. Cy3 serves as negative control. (C) The cytotoxicity of PD-Cy3 was determined by WST-1 assay. All data are presented as the mean ± SD; $^{**}P < 0.01$; $^{**}P < 0.01$; $^{***}P < 0.001$.

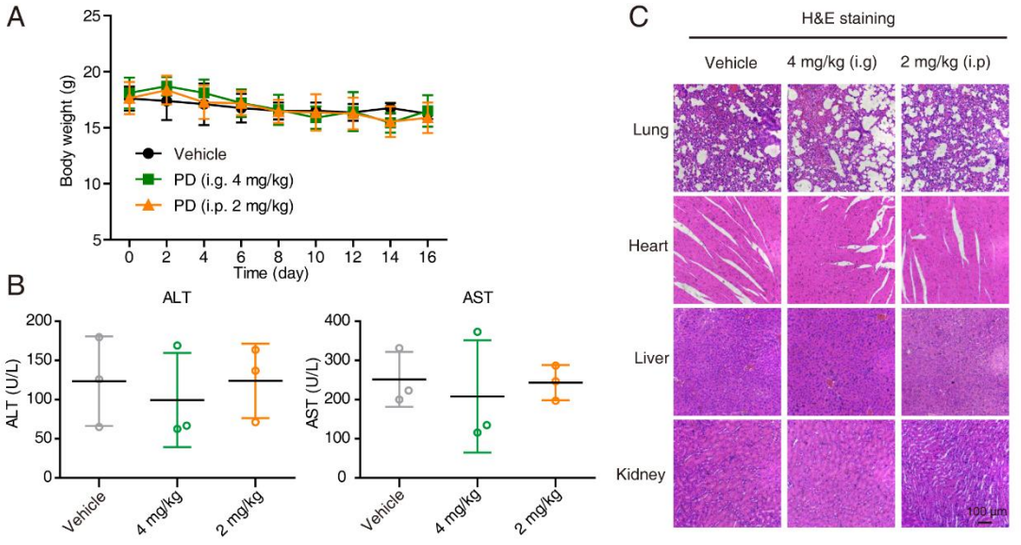

Figure S2. Evaluation of the toxic effect of PD on animal. (A) Body weight of nude mice during the experimental period. (B) Serum ALT and AST levels in PD-treated mice were compared with the vehicle-treated mice (n = 3). (C) Hematoxylin and eosin (H&E) staining of the lung, heart, liver and kidney collected from the mice of the treatment groups and the control group. All data are presented as the mean ± SD.

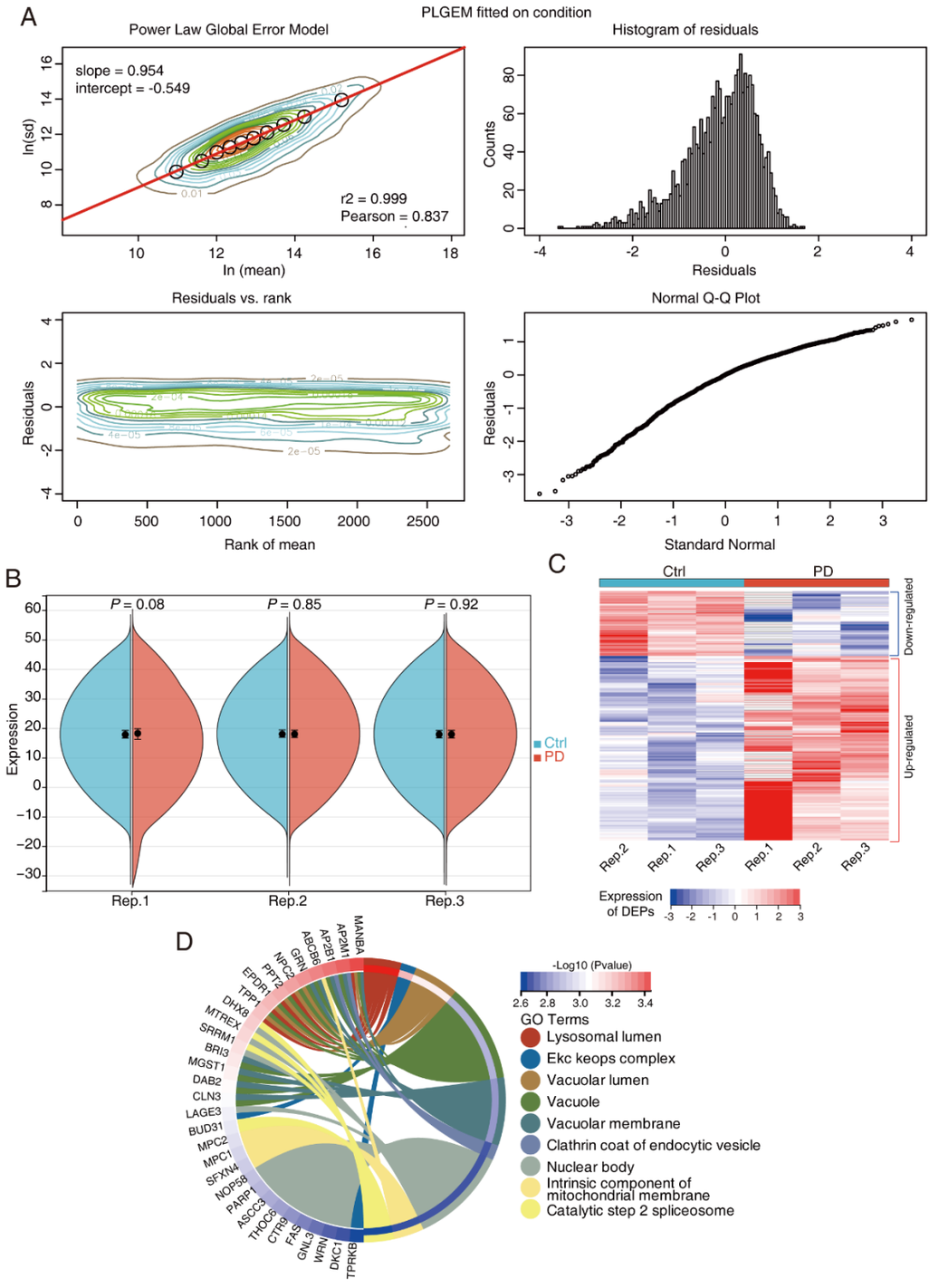

Figure S3. Proteomic analysis of PD-regulated DEPs. (A) The proteins were subjected to a PLGEM model. PLGEM fitting of the abundance of PD-regulated proteins. Histogram of residuals of identified proteins. Residual distribution along

with the rank of mean abundances. Q–Q plot of the residual versus standard normal. (B) Violin plot analysis comparing the distribution of the quantified proteins in the control and PD groups from three biological replicates. The red group represents the PD groups, whereas the blue group represents the control groups. (C) Heatmap showing the expression of DEPs including upregulated proteins and downregulated proteins. (D) GO (cellular components) enrichment analysis of the 247 up-regulated proteins in PD group.

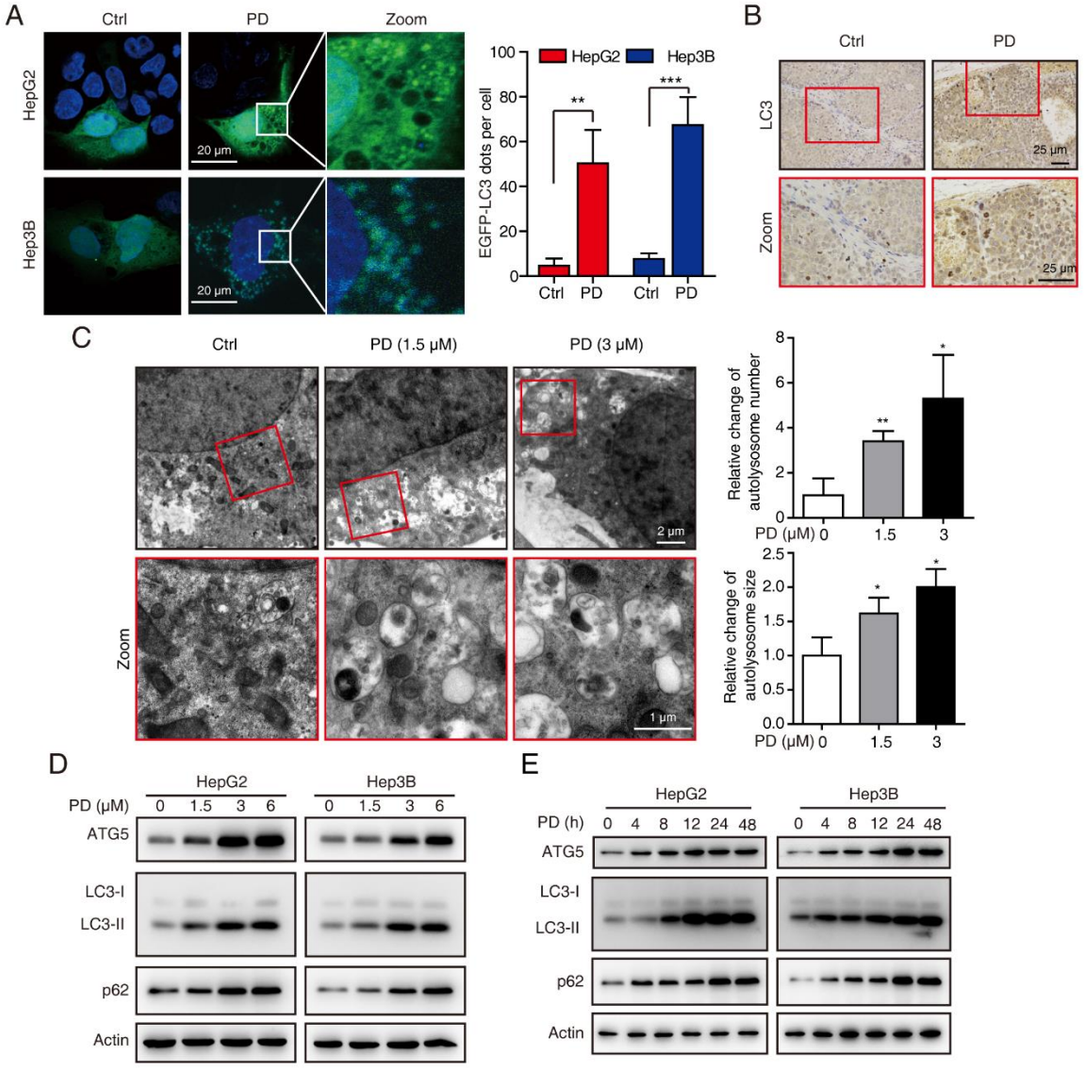

Figure S4. PD triggers the accumulation of autophagosomes in HCC cells. (A) Effect of PD on EGFP-LC3 puncta examined by confocal microscopy. At least 30 cells were counted for analyzing the number of EGFP-LC3 dots in each

condition. (B) IHC staining for LC3 in xenograft tumor tissues from PD (i.p. 2 mg/kg)- and vehicle-treated mice. (C) TEM was performed to compare the morphology of autophagosomes in HepG2 treated with different concentrations of PD for 24 h, the relative number of autophagosomes and the diameter of lysosomes were statistically analyzed, respectively. All data are presented as the mean ± SD; $^{*}P < 0.05$; $^{**}P < 0.01$; $^{***}P < 0.001$. (D) Western blot analysis of the expressions of ATG5, LC3I/II and p62 in the HCC cells treated with PD (0-6 μM, 24 h). (E) Western blot analysis of the expressions of ATG5, LC3I/II and p62 in the HCC cells treated with PD (3 μM) for indicated time points.

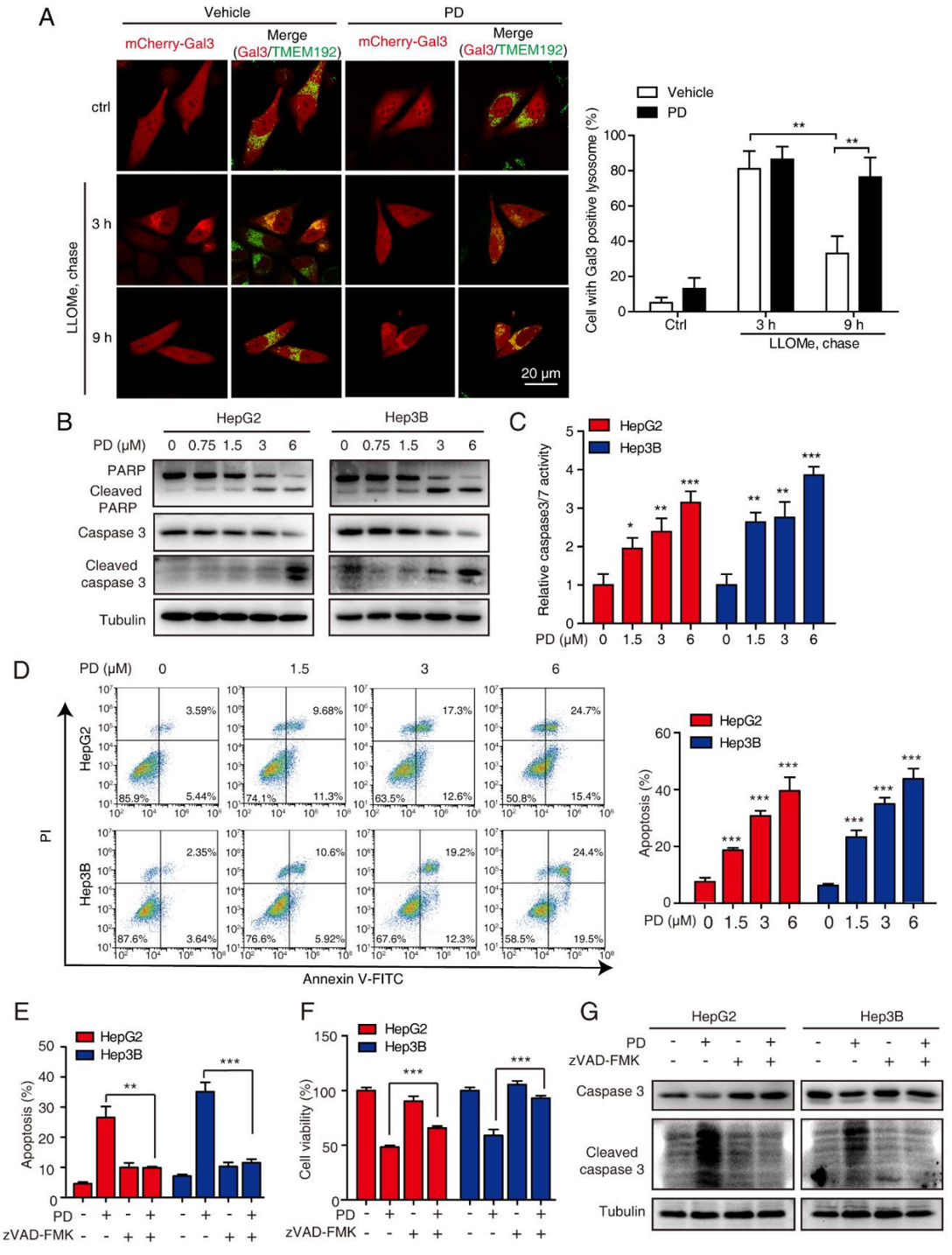

Figure S5. PD impairs the lysosome clearance ability accompanied with apoptosis-like LCD in HCC cells. (A) HepG2 cells with or without PD (1.5 μM) treatment were LLOMe-treated for 1 h and released for indicated times. Percentage of cells with Gal3-positive lysosomes were quantified for three independent experiments. Data were presented as the mean ±

standard deviation; $^{**}P < 0.01$; (B) Western blot analysis of pro-caspase 3, cleaved-caspase 3, pro-PARP and cleaved-PARP expressions in HepG2 and Hep3B cells treated with indicated concentrations of PD for 24 h. (C, D) HCC cells were treated with indicated concentrations of PD for 24 h, the apoptotic cells were detected by caspase-3/7 activity assay (C) and Annexin V-FITC/PI double staining assay (D) using flow cytometry. (E-G) HCC cells were treated with 3 μM PD in the presence or absence of zVAD-FMK (10 μM), then apoptotic cells were analyzed by flow cytometry (E), the cell viability was determined by WST-1 assay (F), the apoptotic markers including pro-caspase 3 and cleaved-caspase 3 were analyzed by western blotting (G). Data are presented as the mean ± SEM for (C-F); $^{*}P < 0.05$; $^{**}P < 0.01$; $^{***}P < 0.001$.

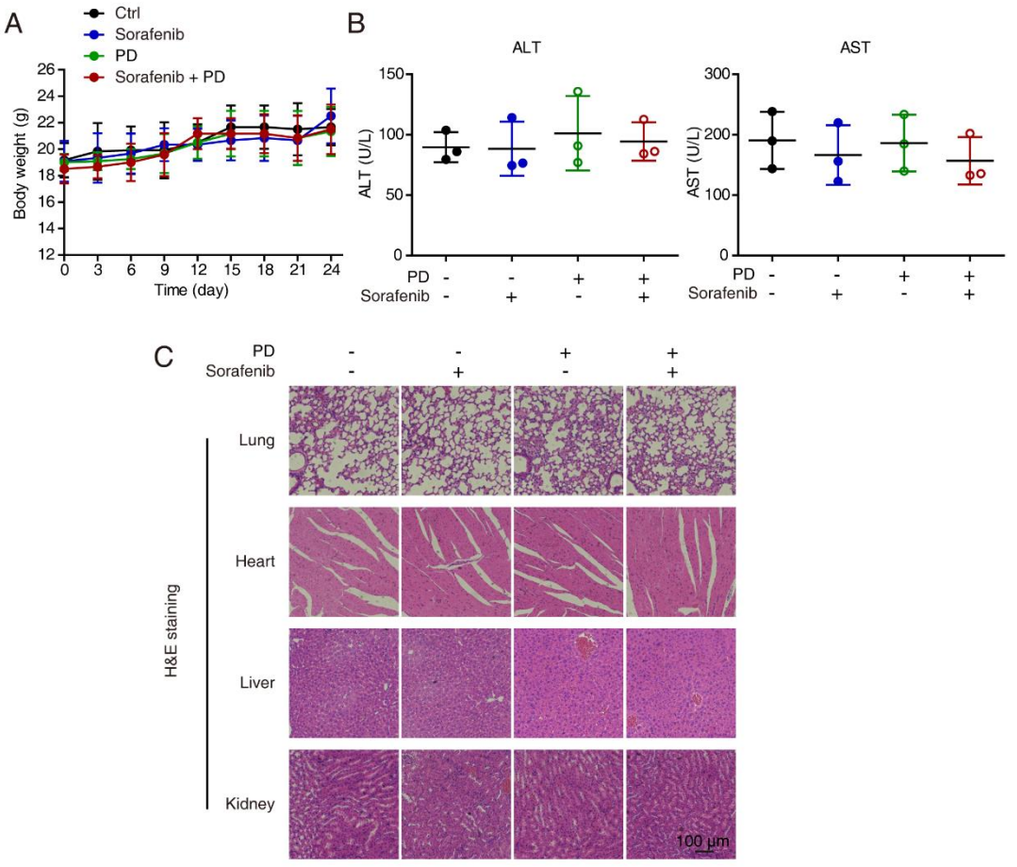

Figure S6. Evaluation of the toxic effect of PD and sorafenib on xenograft model. (A) Body weight of nude mice during the experimental period (n = 6). (B) Serum ALT and AST levels in PD and/or sorafenib-treated mice were compared with the vehicle-treated mice (n=3). (C) Hematoxylin and eosin (H&E) staining of the lung, heart, liver and kidney collected from the mice of the treatment groups and the control group. All data are presented as the mean ± SD.

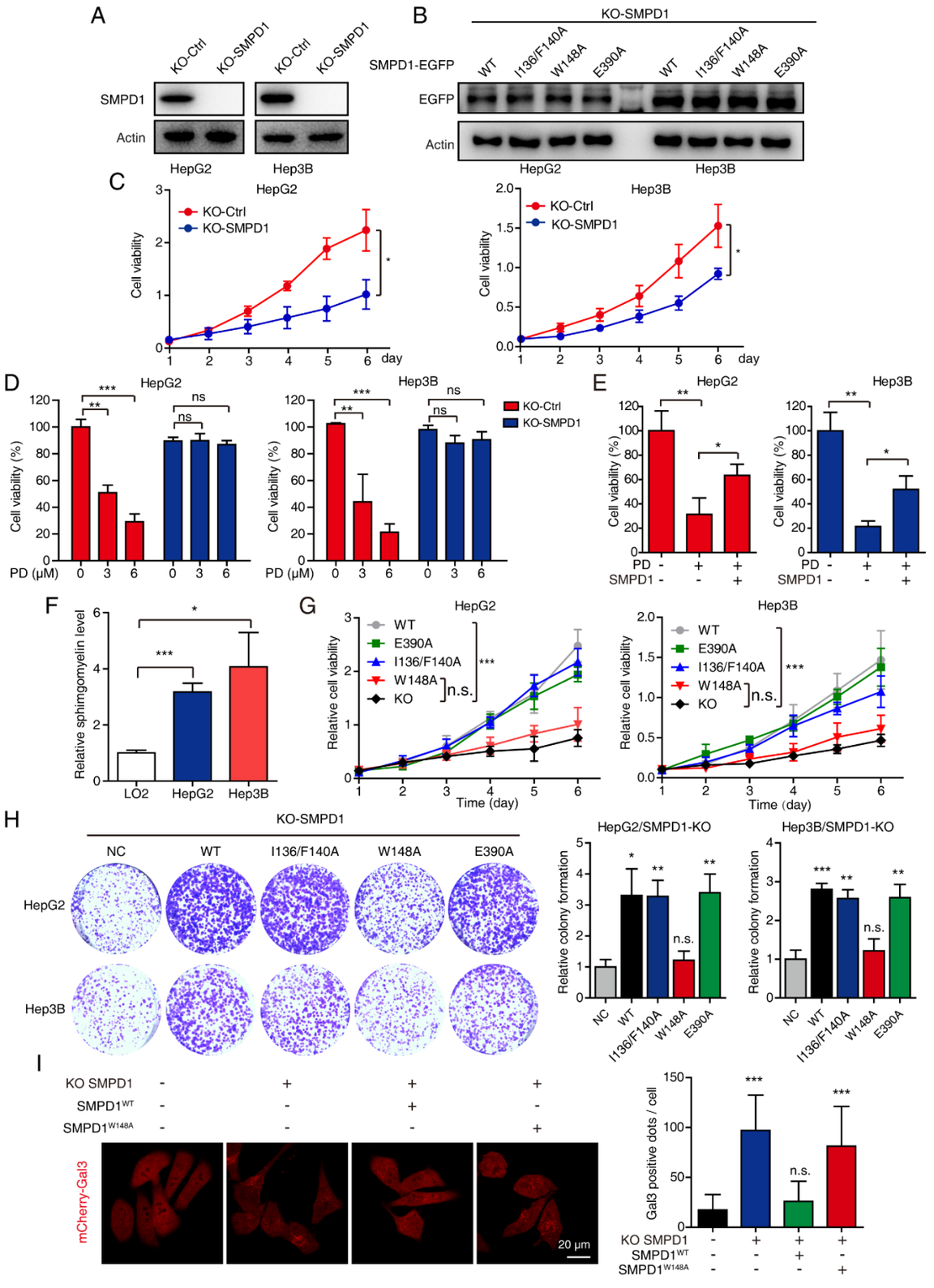

Figure S7. The effect of SMPD1 knockout and SMPD1 mutations on tumor proliferation. (A) SMPD1 was successfully

knocked out (KO) in HepG2 and Hep3B, as detected by western blotting. (B) SMPD1-KO cells were reintroduced with GFP-tagged $SMPD1^{WT}$, $SMPD1^{I136A/F140A}$, $SMPD1^{W148A}$ or $SMPD1^{E390A}$, and the expression of SMPD1-GFP was detected by western blotting. (C) The cell proliferation in the both HCC cells with or without SMPD1 knockout was compared by WST-1 assay. (D) The HepG2 and Hep3B with or without SMPD1 knockout were treated with indicated concentrations of PD for 24 h, the cell viability was then determined by WST-1 assay. (E) The cell viability of HepG2 and Hep3B cells with indicated treatment was determined by WST-1 assay. (F) The cellular sphingomyelin level in HepG2, Hep3B and LO2 cells were measured by using fluorimetric sphingomyelin assay kit. (G) Cell viability of HCC cells with different SMPD1 mutants compared to SMPD1-KO. (H) Colony formation assay was performed to determine the abilities to form colonies of the indicated cell lines. (I) The lysosomal injury in HepG2 cells with SMPD1-KO, $SMPD1^{WT}$ and $SMPD1^{W148A}$ were detected by Gal3 imaging. At least 30 cells were counted for analyzing the number of Gal3 dots in each condition. All data are presented as the mean ± SD; $^{*}P < 0.05$; $^{**}P < 0.01$; $^{***}P < 0.001$; n.s., no significance.

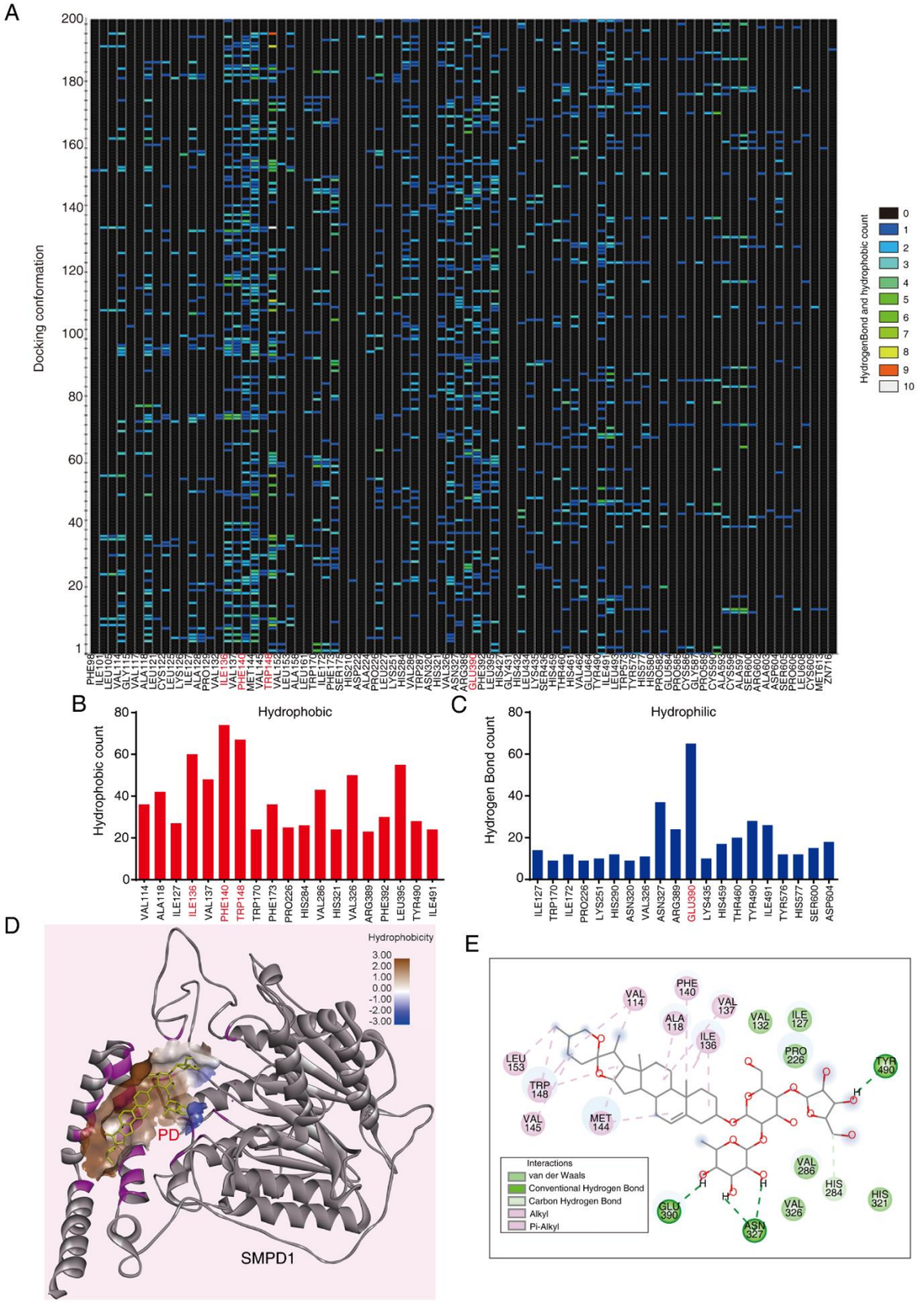

Figure S8. Analysis of binding sites of PD on SMPD1. (A) Heatmap showing 200 possible docking conformations of PD

on SMPD1, the residues with high docking count were shown in red. The hydrophobic count (B) and hydrogen bond count (C) were respectively shown in bar chart. (D) The hydrophily and hydrophobicity of surface groove of SMPD1 occupied by PD were analyzed by Discovery Studio software. (E) 2D diagram showing the interactions between PD and SMPD1 residues, the formed bonds were presented by indicated colors.

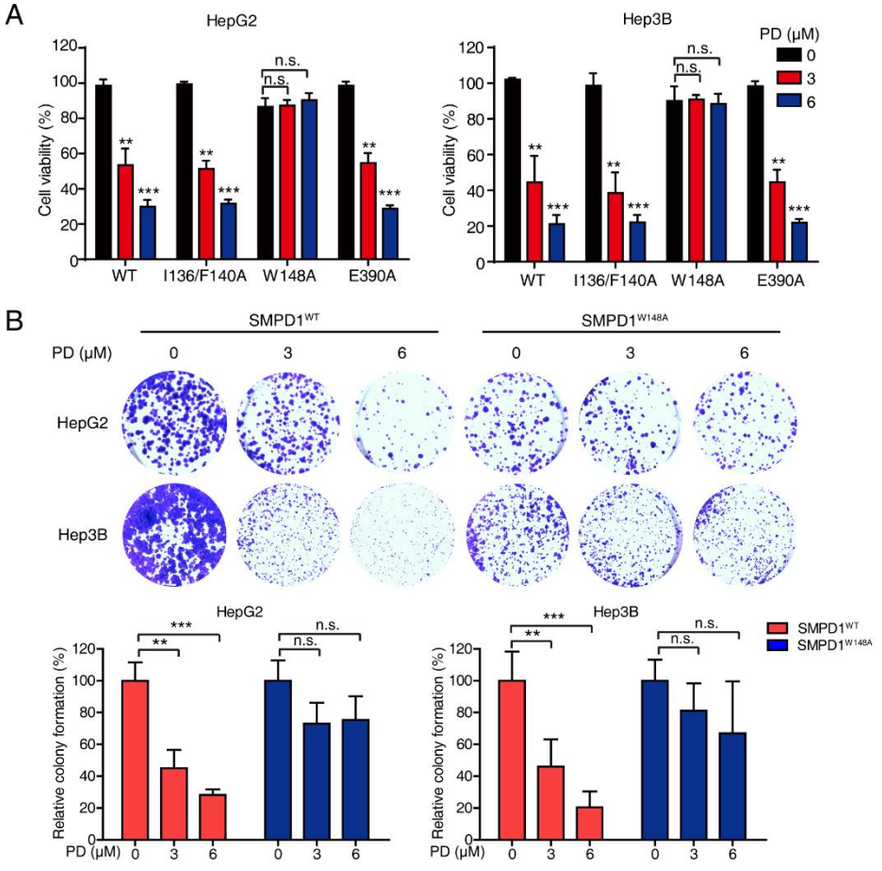

Figure S9. The effect of SMPD1 mutations in response to PD stimuli. (A) SMPD1-KO cells reintroducing $SMPD1^{WT}$, $SMPD1^{I136/F140A}$, $SMPD1^{W148A}$ or $SMPD1^{E390A}$ were treated with indicated concentrations of PD, and the cell proliferation ability was detected by WST-1 assay. (B) SMPD1-KO cells with reintroduced $SMPD1^{WT}$ or $SMPD1^{W148A}$ were treated with indicated concentrations of PD, and the colony formation assays were performed. All data are presented as the mean ± SD; $^{*}P < 0.05$; $^{**}P < 0.01$; $^{***}P < 0.001$; n.s., no significance.

Table S1. Correlation between TMEM192 expression levels and clinicopathological parameters in 80 cases of HCC.

Variable	n	Low TMEM192	High TMEM192	*P* value
Age (years)				0.362
≤55	35	18	17	
>55	44	17	27	
Gender				0.779
Female	16	6	10	
Male	64	29	35	
T-Stage				**0.0122**
1/2	39	21	18	
3/4	27	6	21	
N-Stage				1.000
N0	79	35	44	
N1-2	1	0	1	
M-Stage				0.2524
M0	77	35	42	
M1	3	0	3	
Pathologic stage				**0.0018**
Stages I & II	41	25	16	
Stages III & IV	39	10	29	

Table S2. 14 known compounds for building the lysosomotropic pharmacophore.

Compound name	Molecular formula	SMILES	References
Amiodarone	C25H29I2NO3	CCCCC1=C(C2=CC=CC=C2O1)C(=O)C3=CC(=C(C(=C3)I)OCCN(CC)CC)I	[1]
Astemizole	C28H31FN4O	COC1=CC=C(C=C1)CCN2CCC(CC2)NC3=NC4=CC=CC=C4N3CC5=CC=C(C=C5)F	[2]
Bepridil	C24H34N2O	CC(C)COCC(CN(CC1=CC=CC=C1)C2=CC=CC=C2)N3CCCC3	[3]
Chlorpromazine	C17H19ClN2S	CN(C)CCCN1C2=CC=CC=C2SC3=C1C=C(C=C3)Cl	[4]
Chloroquine	C18H26ClN3	CCN(CC)CCCC(C)NC1=C2C=CC(=CC2=NC=C1)Cl	[5]
Clomifene citrate	C32H36ClNO8	CCN(CC)CCOC1=CC=C(C=C1)C(=C(C2=CC=CC=C2)Cl)C3=CC=CC=C3.C(C(=O)O)C(CC(=O)O)(C(=O)O)	[6]
Loratadine	C22H23ClN2O2	CCOC(=O)N1CCC(=C2C3=C(CCC4=C2N=CC=C4)C=C(C=C3)Cl)CC1	[2]
(-)-Mefloquine	C17H16F6N2O	C1CCNC(C1)C(C2=CC(=NC3=C2C=CC=C3C(F)(F)F)C(F)(F)F)O	[7]
Quinacrine	C23H30ClN3O	CCN(CC)CCCC(C)NC1=C2C=C(C=CC2=NC3=C1C=CC(=C3)Cl)OC	[8]
Sertraline	C17H17Cl2N	CNC1CCC(C2=CC=CC=C12)C3=CC(=C(C=C3)Cl)Cl	[9]
Siramesine	C30H31FN2O	C1CN(CCC12C3=CC=CC=C3CO2)CCCCC4=CN(C5=CC=CC=C54)C6=CC=C(C=C6)F	[10]
Tamoxifen	C26H29NO	CCC(=C(C1=CC=CC=C1)C2=CC=C(C=C2)OCCN(C)C)C3=CC=CC=C3	[11]
Terfenadine	C32H41NO2	CC(C)(C)C1=CC=C(C=C1)C(CCCN2CCC(CC2)C(C3=CC=CC=C3)(C4=CC=CC=C4)O)O	[9]
Trimipramine	C20H26N2	CC(CN1C2=CC=CC=C2CCC3=CC=CC=C31)CN(C)C	[12]

Table S3. Differentially expressed proteins regulated by PD

Supplemental References

1. Sagini, K., Buratta, S., Delo, F., Pellegrino, R. M., Giovagnoli, S., Urbanelli, L., and Emiliani, C. (2021). Drug-Induced Lysosomal Impairment Is Associated with the Release of Extracellular Vesicles Carrying Autophagy Markers. Int J Mol Sci. *22*.
2. Ellegaard, A. M., Dehlendorff, C., Vind, A. C., Anand, A., Cederkvist, L., Petersen, N. H. T., Nylandsted, J., Stenvang, J., Mellemgaard, A., Osterlind, K., et al. (2016). Repurposing Cationic Amphiphilic Antihistamines for Cancer Treatment. EBioMedicine. *9*, 130-139.
3. Capell, A., Liebscher, S., Fellerer, K., Brouwers, N., Willem, M., Lammich, S., Gijselinck, I., Bittner, T., Carlson, A. M., Sasse, F., et al. (2011). Rescue of progranulin deficiency associated with frontotemporal lobar degeneration by alkalizing reagents and inhibition of vacuolar ATPase. J Neurosci. *31*, 1885-1894.
4. Kubo, M., and Hostetler, K. Y. (1985). Mechanism of cationic amphiphilic drug inhibition of purified lysosomal phospholipase A1. Biochemistry. *24*, 6515-6520.
5. Mauthe, M., Orhon, I., Rocchi, C., Zhou, X., Luhr, M., Hijlkema, K. J., Coppes, R. P., Engedal, N., Mari, M., and Reggiori, F. (2018). Chloroquine inhibits autophagic flux by decreasing autophagosome-lysosome fusion. Autophagy. *14*, 1435-1455.
6. Li, W., Lin, J., Shi, Z., Wen, J., Li, Y., Liu, Z., and Diao, A. (2019). Clomiphene citrate induces nuclear translocation of the TFEB transcription factor and triggers apoptosis by enhancing lysosomal membrane permeabilization. Biochem Pharmacol. *162*, 191-201.
7. Ginsburg, H., and Krugliak, M. (1988). Effects of quinoline-containing antimalarials on the erythrocyte membrane and their significance to drug action on Plasmodium falciparum. Biochem Pharmacol. *37*, 2013-2018.
8. Balasubramanian, A., Teramoto, T., Kulkarni, A. A., Bhattacharjee, A. K., and Padmanabhan, R. (2017). Antiviral activities of selected antimalarials against dengue virus type 2 and Zika virus. Antiviral Res. *137*, 141-150.
9. Kornhuber, J., Tripal, P., Reichel, M., Terfloth, L., Bleich, S., Wiltfang, J., and Gulbins, E. (2008). Identification of new functional inhibitors of acid sphingomyelinase using a structure-property-activity relation model. J Med Chem. *51*, 219-237.
10. Ostenfeld, M. S., Hoyer-Hansen, M., Bastholm, L., Fehrenbacher, N., Olsen, O. D., Groth-Pedersen, L., Puustinen, P., Kirkegaard-Sorensen, T., Nylandsted, J., Farkas, T., et al. (2008). Anti-cancer agent siramesine is a lysosomotropic detergent that induces cytoprotective autophagosome accumulation. Autophagy. *4*, 487-499.
11. Soldati, C., Lopez-Fabuel, I., Wanderlingh, L. G., Garcia-Macia, M., Monfregola, J., Esposito, A., Napolitano, G., Guevara-Ferrer, M., Scotto Rosato, A., Krogsaeter, E. K., et al. (2021). Repurposing of tamoxifen ameliorates CLN3 and CLN7 disease phenotype. EMBO Mol Med. *13*, e13742.
12. Inagaki, M., Katsumoto, T., Nanba, E., Ohno, K., Suehiro, S., and Takeshita, K. (1993). Lysosomal glycosphingolipid storage in chloroquine-induced alpha-galactosidase-deficient human endothelial cells with transformation by simian virus 40: in vitro model of Fabry disease. Acta Neuropathol. *85*, 272-279.